DOI: ADD DOINUMBER HERE

A software suite for orbit determination in Space Surveillance and Tracking applications

Marco Felice Montaruli[⋆†], *Giovanni Purpura*[⋆], *Riccardo Cipollone*[⋆], *Andrea De Vittori*[⋆], *Luca Facchini*[⋆], *Pierluigi Di Lizia*[⋆], *Mauro Massari*[⋆], *Moreno Peroni*[◇], *Alessandro Panico*[◇], *Andrea Cecchini*[◇], *Marco Rigamonti*[◇]
[⋆]*Politecnico di Milano*
Via G. La Masa 34, 20156, Milan, Italy
[◇]*Aeronautica Militare - Reparto Sperimentale di Volo*
Via Pratica di Mare 45, 00071, Pomezia (RM), Italy
marcofelice.montaruli@polimi.it · giovanni.purpura@mail.polimi.it · riccardo.cipollone@polimi.it · andrea.devittori@polimi.it · luca.facchini@polimi.it · pierluigi.dilizia@polimi.it · mauro.massari@polimi.it · [†]Corresponding author

Abstract

The in-orbit overpopulation is currently fostering Space Surveillance and Tracking (SST) related applications, in which ground-based sensors (optical and radar) are typically used. This paper presents the orbit determination functions provided by the novel Italian SST Operation Centre (ISOC) Suite. First, a statistical index is computed to assess the measurements correlation to a catalogued object. If it is successful, the object predicted orbit is refined through either batch or sequential filters, otherwise dedicated methodologies are exploited to first estimate the orbital state of the target. Finally, the paper assesses ISOC performances both in terms of synthetic and real data.

1. Introduction

In the last decades, in orbit population has become a problem of utmost importance for space agencies and institutions worldwide. The two most populated regions are Low Earth Orbit (LEO) and Geostationary Orbit (GEO). Among orbiting objects, just a small fraction is represented by co-operative satellites and the main part is represented by space debris, which include inactive satellites, rocket bodies, and fragments of all sizes.[1] Space debris represent a threat to space activities (in orbit collision risk, for instance) and so different strategies have been implemented to guarantee safe operations. For this purpose, an international commitment is currently taking place in the Space Surveillance and Tracking (SST) field. Europe deals with this topic through two programmes: the European Space Agency (ESA) Space Situational Awareness (SSA) programme[2] and the European Space Surveillance and Tracking (EUSST) framework.[3] The latter groups European national agencies and institutions and is in charge of carrying out the following services: conjunction analysis, fragmentation analysis and re-entry prediction. These services exploit measurements obtained through ground-based sensors, which are optical telescopes (they provide highly accurate angular track), radars (in addition to angles, they provide either range or doppler shift measurements or both) and lasers (they provide extremely precise range measurements).
Italy is involved in EUSST programme through Italian Space Agency (ASI), Astrophysics National Institute (INAF) and Italian Airforce (AM), and it is in charge of reentry and fragmentation services. For this reason efficient and reliable tools shall be designed to process observation data. Within this framework, the Italian SST Operational Centre (ISOC) has recently upgraded its system to ISOC Suite, an integrated platform providing multiple functions and services in the SST domain. It is a web-based platform giving users the ability to connect and use the system both locally and remotely. The software has been designed and implemented in partnership with industry and academia. The present work describes the orbit determination module developed for the ISOC Suite thanks to a collaboration involving the Italian Air Force, Leonardo Company and Politecnico di Milano. After the definition of the software architecture, its prototypal version has been developed and then translated to C++ language to be used in the operational environment, guaranteeing the highest performances in terms of computational times.
One of the key points is to correlate measurements, provided by sensor network in the form of TDM,[4] to catalogued objects and to perform orbit determination (OD). To determine the orbital state of an observed object, sensor measurements can be processed in two ways, depending on whether the data refer to a catalogued object or not.
In the catalogued case, orbital state predictions of the object are available. These are refined using the measurements

and this process is known as Refined Orbit Determination (ROD). It is typically based on larger amounts of available data and can be distinguished between batch methods (for predictions without uncertainty), in which the complete data set acquired over a certain time horizon is used to find a solution, and sequential methods (for predictions with uncertainty), in which measurement information is processed as soon as it is available. Both batch and sequential methods are iterative and require sufficiently good initial guesses. In addition to the position and the velocity, these algorithms can also estimate object physical parameters (such as the ballistic coefficient).
For uncatalogued objects instead, no prediction is available and only measurements can be exploited. In this case, an Initial Orbit Determination (IOD) is performed, through dedicated methodologies. In this context, the most reliable methodologies usually estimate orbital position and velocity only.
In an operational scenario, the measurements are recorded and then a correlation procedure is performed to link the measurements to a catalogued object, which is propagated towards the observation epochs. If the correlation is successful, a ROD is run, otherwise an IOD procedure is performed. A similar process can be run to check the compatibility of the OD result with respect to the input measurements, as deepened in Sec. 3.

The objective of this work is to present the software suite for orbit determination embedded in ISOC, by assessing its performance both in terms of synthetic and real data. The paper is organized as follows. First an overview of ISOC suite is provided and the mathematical theory of the process is discussed. Then a numerical analysis is carried out to validate the tool. Finally, the algorithm performance is assessed through operational real case scenarios.

2. Italian SST Operations Centre

ISOC was originally established in 2014 and operated by the military personnel of the Flight Test Wing of the Italian Air Force. Currently, the operational activities are lead by the the Air and Space Operations Command, whereas the Flight Test Wing is responsible for Research and Development tasks. The ISOC Suite is a complex system that was originally developed to support Space Surveillance and Tracking tasks, but it is currently evolving towards a broader awareness of the space scenario, to enhance the national security for both civil and military applications. ISOC is also included in the EUSST framework, supporting the service listed below:

- Re-entry (RE): prime responsible for the analysis of uncontrolled re-entry in low atmosphere for large and dangerous objects.
- Fragmentation (FG): prime responsible for the analysis of in-orbit fragmentation as consequence of satellite break-ups or collisions.
- Conjunction Analysis (CA): cold redundant operational center for the analysis of the collision probability and geometry for conjunction events.

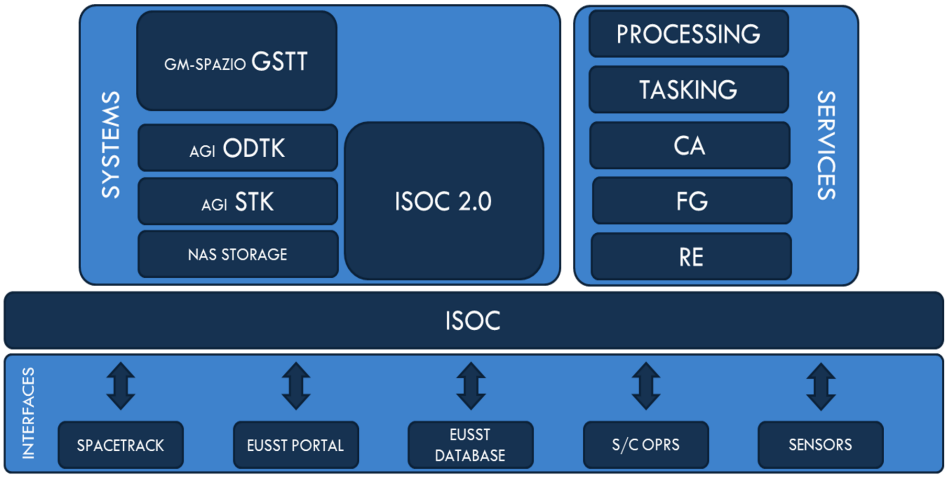

Figure 1: ISOC Architecture

ISOC Suite is used to support the above-mentioned services, whose high level architecture is represented in Fig. 1. The main inputs of the suite are provided by national sensors, consortium observations, European observation catalogue (DCED) along with available public sources. The inner part of the system is based on commercial on the shelf (COTS)

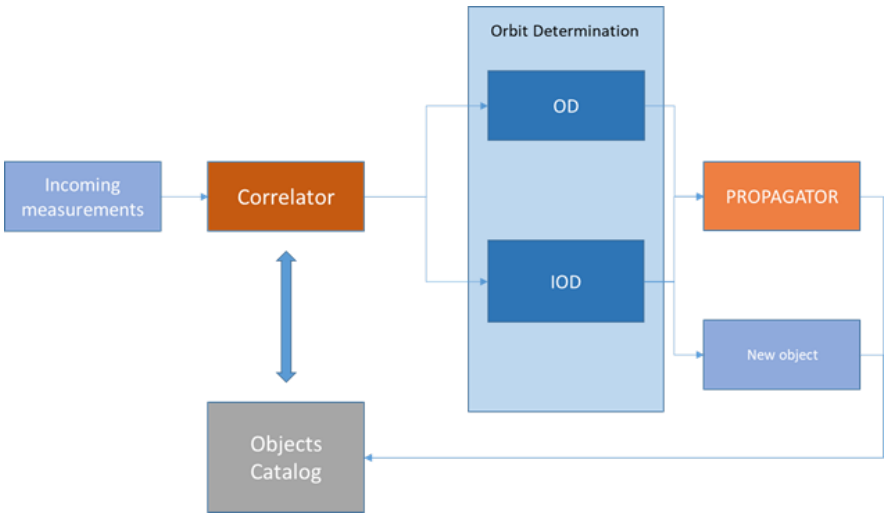

Figure 2: Correlation and Orbit Determination work-flow

and proprietary software. The system output are the services shown in the right part of Fig. 1. A functional part of the entire system is the correlation and the orbit determination process, that could be assured by the suite described in this document. The logical workflow is depicted in Fig.2 and it is described in detail in the next sections.

3. Correlation process

To correlate measurements to a catalogued object, a statistical correlation index is computed using the concept of Mahalanobis distance. Assuming a normal distribution, the acquired measurements, at each observation epoch t_k, can be expressed as $\boldsymbol{Y}(t_k) \sim \mathcal{N}\left(\boldsymbol{\mu_y}(t_k), \boldsymbol{P_y}\right)$, where $\boldsymbol{P_y}$ is constant and is defined based on sensor accuracy. $\boldsymbol{Y}$ has dimension $\mathrm{N}_y \mathrm{x} \mathrm{N}_{obs}$, where N_{obs} is the number of observation epochs and N_y depends on the acquired measurements (2 for the optical case, 3 or 4 for a radar, depending on whether slant range or Doppler shift, or both values are acquired, and so on). In order to verify the correlation status of a generic catalogued orbital state $\boldsymbol{X} \sim \mathcal{N}\left(\boldsymbol{\mu_x}, \boldsymbol{P_x}\right)$, this can be propagated (by using SGP4,[5] for instance) up to the observation epochs and then projected in the measurement space, according to an Unscented Transformation (UT).[6] This operation results in the predicted measurement set $\tilde{\boldsymbol{Y}}(t_k) \sim \mathcal{N}\left(\tilde{\boldsymbol{\mu}}_{\boldsymbol{y}}(t_k), \tilde{\boldsymbol{P}}_{\boldsymbol{y}}(t_k)\right)$, where, differently from $\boldsymbol{P_y}$, $\tilde{\boldsymbol{P}}_{\boldsymbol{y}}$ depends on the observation epoch t_k considered.
For each observation epoch t_k, the Mahalanobis distance is computed as:

$$\xi(t_k) = \left\{\tilde{\boldsymbol{\mu}}_{\boldsymbol{y}}(t_k) - \boldsymbol{\mu_y}(t_k)\right\}^T \left\{\boldsymbol{P_y} + \tilde{\boldsymbol{P}}_{\boldsymbol{y}}(t_k)\right\}^{-1} \left\{\tilde{\boldsymbol{\mu}}_{\boldsymbol{y}}(t_k) - \boldsymbol{\mu_y}(t_k)\right\} \tag{1}$$

And it is divided by the inverse of the chi-square cumulative distribution function for a probability of 99.8 % and a N_y number of degrees of freedom:

$$\zeta(t_k) = \frac{\xi(t_k)}{\bar{\chi}^2} \tag{2}$$

Finally, the correlation index $\bar{\zeta}$ is selected as the mean value of all the $\zeta(t_k)$ computed along the observation window. If this quantity satisfies a given threshold τ, the measurements can be considered correlated to the catalogued orbital state $\boldsymbol{X}$. To respect the 3-σ level of probability, the threshold τ shall be theoretically set equal to 1. However, for noisy and not accurate measurements (such as in real case scenario), it can occur that such a quantity is not respected even for correct correlations, and τ shall be relaxed accordingly. It takes place, for instance, when the measurement noise exceeds the declared accuracy (information included in the covariance matrix $\boldsymbol{P_y}$), or when its distribution is not Gaussian. This matter is further discussed in Sec. 7.
Given a catalogue and a TDM containing observables, the ISOC Suite correlation process is performed as follows:

1. Propagate all the catalogued objects up to the TDM observation epochs, and project the orbital states in the measurements space, obtaining, at each time t_k, the predicted measurements $\tilde{\boldsymbol{\mu}}_{\boldsymbol{y}}(t_k)$.

2. Filter out objects with an angular distance at initial and final TDM observation epochs greater than a threshold (set by the user).

3. For the remaining objects, at each observation epoch t_k compute Eq. 1 and Eq. 2, and then the correlation index $\overline{\zeta}$.

4. The process correlates the measurements to the object featuring the smallest correlation index.

An analogous procedure is here used also to define an index which assesses the compatibility of the OD results with the measurements adopted in the estimation process. From the resulting mean $\boldsymbol{\mu_x}$ and covariance $\boldsymbol{P_x}$ at the OD reference epoch, the related synthetic measurements $\tilde{\boldsymbol{Y}}(t_k)$ are computed at each t_k. Then, Eq. 1 and Eq. 2 are evaluated, and the mean correlation index $\bar{\zeta}$ is computed. Finally an OD result is considered to be satisfactory if $\overline{\zeta} < \tau$, where the same considerations as above apply to τ.

4. Refined Orbit Determination

In ROD processes, an orbital state prediction $\boldsymbol{X_0} \sim \mathcal{N}(\boldsymbol{\mu_{x0}}, \boldsymbol{P_{x0}})$ is refined based on the acquired measurements $\boldsymbol{Y} \sim \mathcal{N}\left(\boldsymbol{\mu_y}, \boldsymbol{P_y}\right)$. Generally, either batch filters like the Non-linear Least Squares, or sequential filter like the Kalman Filters are used.[7] The former can refine the orbital state prediction also when the covariance $\boldsymbol{P_{x0}}$ is not known, while the latter cannot.
ISOC exploits Non-linear Least Squares (as batch filter) and Unscented Kalman Filters (as sequential filter). The latter is used when a covariance is associated to the prediction, while the former when it is not, and the software is designed to automatically select the correct routine based on the input data.

Non-linear Least Squares[7]
Generally speaking, the Non-linear Least Squares methods seek to refine an orbital state $\boldsymbol{\mu_{x0}}$ (of dimension N_x), defined at time $\hat{t}$ and considered as process first guess, by searching for the mean orbital state $\boldsymbol{\mu_x}$ as that value that minimizes the sum of the squares of the calculated observation residuals.
Let the residual vector be:

$$\boldsymbol{\varepsilon}(\boldsymbol{\mu_x}) = \left(\boldsymbol{\mu_y} - \tilde{\boldsymbol{\mu}}_{\boldsymbol{y}}(\boldsymbol{\mu_x})\right) \tag{3}$$

Of dimension is N_ε=N_{obs}+N_y, where N_{obs} is the observation epochs number and N_y is the dimension of measurement state. Then, $\boldsymbol{\mu_y}$ is the set of observation data (mapped in the measurements space) and $\tilde{\boldsymbol{\mu}}_{\boldsymbol{y}}$ is the synthetic measurements set, retrieved from $\boldsymbol{\mu_{x0}}$ according to the procedure described in Sec. 3. The process searches for the value of $\boldsymbol{\mu_x}$ which minimizes the following performance index:

$$h(\boldsymbol{\mu_x}) = \frac{1}{2}\boldsymbol{\varepsilon}(\boldsymbol{\mu_x})^T\,\boldsymbol{\varepsilon}(\boldsymbol{\mu_x}) \tag{4}$$

Note that Eq. 4 is a quadratic function of $\boldsymbol{\mu_x}$, and, as a consequence, the expression has a unique minimum when:

$$\frac{\partial h}{\partial \boldsymbol{\mu_x}} = 0 \quad \text{and} \quad \delta\boldsymbol{\mu_x}^T \frac{\partial^2 h}{\partial \boldsymbol{\mu_x}^2}\delta\boldsymbol{\mu_x} > 0 \tag{5}$$

for $\delta\boldsymbol{\mu_x} \neq 0$. The second condition of Eq. 5 means that $\partial^2 h/\partial\boldsymbol{\mu_x}^2$ is positive defined.
If the process converges, the orbital state $\boldsymbol{X}$ is found, both in terms of the estimated $\boldsymbol{\mu_x}$ and covariance, which is computed as:

$$\boldsymbol{P_x} = \frac{\boldsymbol{\varepsilon}(\boldsymbol{\mu_x})^T\,\boldsymbol{\varepsilon}(\boldsymbol{\mu_x})}{\mathrm{N}_\epsilon - \mathrm{N}_x}\left(\boldsymbol{J}(\boldsymbol{\mu_x})^T\,\boldsymbol{J}(\boldsymbol{\mu_x})\right)^{-1} \tag{6}$$

Where $\boldsymbol{J}(\boldsymbol{\mu_x})$ is the Jacobian of $\boldsymbol{\varepsilon}(\boldsymbol{\mu_x})$ at the solution $\boldsymbol{\mu_x}$.
There are different variations to this scheme, the most remarkable being the weighted Non-linear Least Squares, in which Eq. 4 is modified as:

$$h(\boldsymbol{\mu_x}) = \frac{1}{2}\boldsymbol{\varepsilon}(\boldsymbol{\mu_x})^T\,\boldsymbol{W_y}\,\boldsymbol{\varepsilon}(\boldsymbol{\mu_x}) \tag{7}$$

Where $\boldsymbol{W_y}$ is the matrix weighting the observation errors and usually results from an initial judgment on the accuracy of the observations (the sensor accuracy, for instance), followed by a normalization procedure to scale the weights to values between zero and one.
Even if the Non-linear Least Squares approaches are theoretically exploitable for IOD (starting from a circular first guess, for instance), they are operationally considered just for ROD operations, as an accurate $\boldsymbol{\mu_{x0}}$ is fundamental to get convergence.

Unscented Kalman Filter

An efficient way to perform ROD with a sequential filter is represented by the Unscented Kalman Filter. It is a technique based on the Unscented Transformation without any linearization, and thus provides superior performance with respect to the EKF in nonlinear problems[6,8].

In a ROD operation, let's consider a prediction state $\boldsymbol{X_0} \sim \mathcal{N}(\boldsymbol{\mu_{x0}},\ \boldsymbol{P_{x0}})$ defined at reference time t_0. Its dimension N_x depends on the parameters to update: N_x=6 to refine just the orbital state, N_x=7 if an additional physical parameter (such as the ballistic coefficient) is considered, and so on. Let the ROD measurements set be $\boldsymbol{Y}(t_k) \sim \mathcal{N}\left(\boldsymbol{\mu_y}(t_k),\ \boldsymbol{P_y}\right)$, where $\boldsymbol{\mu_y}(t_k)$ represents the acquired measurements at each observation epoch t_k and $\boldsymbol{P_y}$ the constant covariance defined up to the sensor accuracy.

From $\boldsymbol{X}$, the UT sigma points are created: $\bar{\boldsymbol{\mu}}_{\boldsymbol{x}}(t_0)$. These are propagated up to the first-step observation epoch t_1, resulting in the propagated N_x-dimensional sigma points: $\bar{\boldsymbol{\mu}}_{\boldsymbol{x}}^{\boldsymbol{i}}(t_1|t_0)$ (for the i-th sigma point). Given the non-linear function g which projects an orbital state onto the measurement space, the predicted measurements sigma points can be computed at the first-step observation epoch t_1, whose dimension N_y corresponds to the number of considered measurements: $\bar{\boldsymbol{\mu}}_{\boldsymbol{y}}^{\boldsymbol{i}}(t_1|t_0) = g\left(\bar{\boldsymbol{\mu}}_{\boldsymbol{x}}^{\boldsymbol{i}}(t_1|t_0)\right)$. Then, the augmented sigma point $\bar{\boldsymbol{\mu}}_{\boldsymbol{\xi}}^{\boldsymbol{i}}(t_1|t_0)$ is created, chaining $\bar{\boldsymbol{\mu}}_{\boldsymbol{x}}^{\boldsymbol{i}}$ and $\bar{\boldsymbol{\mu}}_{\boldsymbol{y}}^{\boldsymbol{i}}$:

$$\bar{\boldsymbol{\mu}}_{\boldsymbol{\xi}}^{\boldsymbol{i}}(t_1|t_0) = \begin{bmatrix} \bar{\boldsymbol{\mu}}_{\boldsymbol{x}}^{\boldsymbol{i}}(t_1|t_0) \\ \bar{\boldsymbol{\mu}}_{\boldsymbol{y}}^{\boldsymbol{i}}(t_1|t_0) \end{bmatrix} \tag{8}$$

And its dimension N_ξ turns out to be equal to N_x+N_y.

At this point, the state is retrieved from the sigma points $\bar{\boldsymbol{\mu}}_{\boldsymbol{\xi}}^{\boldsymbol{i}}(t_1|t_0)$ and N_ξ-dimensional state is returned, both in terms of mean $\hat{\boldsymbol{\mu}}_{\boldsymbol{\xi}}(t_1|t_0)$ (dimension N_ξx1) and covariance $\hat{\boldsymbol{P}}_{\boldsymbol{\xi}}(t_1|t_0)$ (dimension N_ξxN_ξ). It is now possible to split $\hat{\boldsymbol{\mu}}_{\boldsymbol{\xi}}(t_1|t_0)$ in:

$$\hat{\boldsymbol{\mu}}_{\boldsymbol{\xi}}(t_1|t_0) = \begin{bmatrix} \hat{\boldsymbol{\mu}}_{\boldsymbol{x}}(t_1|t_0) \\ \hat{\boldsymbol{\mu}}_{\boldsymbol{y}}(t_1|t_0) \end{bmatrix} \tag{9}$$

And $\hat{\boldsymbol{P}}_{\boldsymbol{\xi}}(t_1|t_0)$ in:

$$\hat{\boldsymbol{P}}_{\boldsymbol{\xi}}(t_1|t_0) = \begin{bmatrix} \hat{\boldsymbol{P}}_{\boldsymbol{x}}(t_1|t_0) & \hat{\boldsymbol{P}}_{\boldsymbol{xy}}(t_1|t_0) \\ \hat{\boldsymbol{P}}_{\boldsymbol{xy}}^{\ T}(t_1|t_0) & \hat{\boldsymbol{P}}_{\boldsymbol{y}}(t_1|t_0) \end{bmatrix} \tag{10}$$

Such that the dimensions are N_xx1 for $\hat{\boldsymbol{\mu}}_{\boldsymbol{x}}(t_1|t_0)$, N_yx1 for $\hat{\boldsymbol{\mu}}_{\boldsymbol{y}}(t_1|t_0)$, N_xxN_x for $\hat{\boldsymbol{P}}_{\boldsymbol{x}}(t_1|t_0)$, N_yxN_y for $\hat{\boldsymbol{P}}_{\boldsymbol{y}}(t_1|t_0)$, N_xxN_y for $\hat{\boldsymbol{P}}_{\boldsymbol{xy}}(t_1|t_0)$.

By defining:

$$\hat{\boldsymbol{P}}_{\boldsymbol{e}}(t_1|t_0) = \hat{\boldsymbol{P}}_{\boldsymbol{y}}(t_1|t_0) + \boldsymbol{P_y} \tag{11}$$

The covariance gain as:

$$\boldsymbol{K}(t_1|t_0) = \hat{\boldsymbol{P}}_{\boldsymbol{xy}}(t_1|t_0)\,\hat{\boldsymbol{P}}_{\boldsymbol{e}}(t_1|t_0)^{-1} \tag{12}$$

The orbital state is updated as:

$$\begin{aligned} \boldsymbol{\mu_x}(t_1|t_0) =& \hat{\boldsymbol{\mu}}_{\boldsymbol{x}}(t_1|t_0) + \boldsymbol{K}(t_1|t_0)\left\{\boldsymbol{\mu_y}(t_1) - \hat{\boldsymbol{\mu}}_{\boldsymbol{y}}(t_1|t_0)\right\} \\ \boldsymbol{P_x}(t_1|t_0) =& \hat{\boldsymbol{P}}_{\boldsymbol{\mu}}(t_1|t_0) - \boldsymbol{K}(t_1|t_0)\,\hat{\boldsymbol{P}}_{\boldsymbol{e}}(t_1|t_0)\,\boldsymbol{K}^T(t_1|t_0) \end{aligned} \tag{13}$$

By repeating this procedure for all the conditional estimations $(t_{k+1}|t_k)$ sequentially, up to the final-step observation epoch t_f, the orbital state is updated through the measurements.

It is important to highlight that the sequential filter procedure is possible only if a covariance can be associated to the orbital state. In addition, since the procedure is sequential, it can be performed either forward or backward with respect to the observation timeline, but the result is always associated to the final-step observation epoch considered.

5. Initial Orbit Determination

As illustrated above, no orbital predictions are available for the observed object in the IOD context. As exaplained earlier, in this context the Non-linear Least Squares approaches, theoretically, could still be applied (and would allow to estimate other parameters in addition to position and velocity), but they turn out to be quite unstable, mainly due to the lack of a sufficiently accurate first guess. Thus, alternative methodologies have been developed by the scientific community that are applied depending on the available measurements.

ISOC Suite is designed to automatically recognize the input data. Dedicated routines are present, depending on whether the input TDM is optical, or radar-laser. In this latter case, IOD can be performed only from measurements including angles and slant range.

5.1 Radar IOD

The procedure for radar (and laser) measurements is based on the method described in.[9] Let's consider a set of radar sensor observations $\boldsymbol{Y}(t_k) \sim \mathcal{N}\left(\boldsymbol{\mu_y}(t_k), \boldsymbol{P_y}\right)$ (with dimension 3xN_{obs} and 3x3, respectively), where t_k are the N_{obs} observation epochs, $\boldsymbol{\mu_y}(t_k)$ are the measurements mean value acquired at t_k and $\boldsymbol{P_y}$ is the corresponding covariance and which is derived from the sensor accuracy. This information, together with the time-dependent inertial sensor position $\boldsymbol{s}(t_k)$, can be processed to estimate the object orbital position $\boldsymbol{r}(t_k)$, whose uncertainty is described in terms of a multivariate normal distribution. In particular, the covariance $\boldsymbol{P_r}(t_k)$ can be derived from $\boldsymbol{Y}(t_k)$ with an UT,[6] by projecting the sigma points from the measurements to the inertial space.
The $\boldsymbol{r}(t_k)$ vectors can be grouped in a sngle matrix: $\boldsymbol{Z} = \left(\boldsymbol{r}^T(t_1), \boldsymbol{r}^T(t_2), ..., \boldsymbol{r}^T(t_{\mathrm{N}_{obs}})\right)$. From $\boldsymbol{Z}$, the algorithm proceeds iteratively by modifying the orbital mean state with a fixed-point update process, starting from a first guess $\boldsymbol{\mu_0}$ (obtained with a keplerian circular orbit assumption):

$$\boldsymbol{\mu_x}^j = \boldsymbol{H}(\boldsymbol{\mu_x}^{j-1})\boldsymbol{Z} \tag{14}$$

By defining the j-th residual as $R^j = \max(|\boldsymbol{x}^j - \boldsymbol{x}^{j-1}|)$, the loop goes on as long as $\left(R^j - R^{j-1}\right)/R^j$ is larger than a tolerance τ or the current number of iterations λ is lower than a predefined threshold.
At any iteration j, the matrix $\boldsymbol{H}(\boldsymbol{\mu_x}^{j-1})$ is defined according to $\boldsymbol{f}(\boldsymbol{\mu_x}^{j-1})$ and $\boldsymbol{g}(\boldsymbol{\mu_x}^{j-1})$, which are vectors grouping the Lagrangian coefficients, whose derivations are provided in e.g.:[10]

$$\boldsymbol{H}\left(\boldsymbol{\mu_x}^{j-1}\right) = \frac{1}{\delta}\begin{pmatrix}\boldsymbol{g^T g F} - \boldsymbol{f^T g G} \\ \boldsymbol{f^T f G} - \boldsymbol{f^T g F}\end{pmatrix} \tag{15}$$

where the denominator is:

$$\delta = \left(\boldsymbol{f^T f}\right)\left(\boldsymbol{g^T g}\right) - (\boldsymbol{f^T g})^2 \tag{16}$$

while the auxiliary matrix $\boldsymbol{F}$ (and equivalently $\boldsymbol{G}$) is defined as:

$$\boldsymbol{F} = \begin{pmatrix} f_1 & 0 & 0 & ... & f_{\mathrm{N}_{obs}} & 0 & 0 \\ 0 & f_1 & 0 & ... & 0 & f_{\mathrm{N}_{obs}} & 0 \\ 0 & 0 & f_1 & ... & 0 & 0 & f_{\mathrm{N}_{obs}} \end{pmatrix} \tag{17}$$

where f_k is the Lagrangian coefficient f relative to k-th epoch.
The method converges towards the solution $\boldsymbol{\mu_x}$. The orbital state covariance is finally determined through the linear approximation:

$$\boldsymbol{P_x} = \boldsymbol{H}\left(\boldsymbol{\mu_x}\right)\boldsymbol{P_r}\,\boldsymbol{H^T}\left(\boldsymbol{\mu_x}\right) \tag{18}$$

where $\boldsymbol{P_r} = \mathrm{diag}\left(\boldsymbol{P_r}(t_1), ..., \boldsymbol{P_r}(\boldsymbol{t}_{\mathrm{N}_{obs}})\right)$, and the orbital state $\boldsymbol{X}(\hat{t}) \sim \mathcal{N}\left(\boldsymbol{\mu_x}(\hat{t}), \boldsymbol{P_x}(\hat{t})\right)$ is determined. The epoch $\hat{t}$ is here selected as the first observation epoch.

5.2 Optical IOD

The optical IOD process is structured as a combination of a Gauss method with iterative improvement used to give a first guess (if not otherwise provided by the user), and a Gooding n-measurements version[11] to exploit every intermediate measurements of the observation arc, for the actual orbit estimate. Angular measurement uncertainty is taken into account through UT,[6] considering the estimated orbital state as multivariate normal distribution.
Given a set of optical measurements consisting in a sequence of angular coordinates (α, δ) denoting right ascension and declination of the target, they can be described as a normal distribution $\boldsymbol{Y}(t_k) \sim \mathcal{N}\left(\boldsymbol{\mu_y}(t_k), \boldsymbol{P_y}\right)$ with $k = 1, ..., N_{obs}$, where N_{obs} represents the number of observation epochs, $\boldsymbol{\mu_y}(t_k)$ is the measurement mean values acquired at t_k, $\boldsymbol{P_y}$ the associated covariance, derived from the declared sensor accuracy. This information can be combined with range and inertial station position (which varies across the observation) to retrieve the target position using:

$$\mathbf{r} = \mathbf{R} + \rho\,\mathbf{s} \tag{19}$$

where $\mathbf{r}$ denotes the target position, ρ represents the range while $\mathbf{s}$ is defined as:

$$\mathbf{s} = \left(\cos\alpha\,\cos\delta, \sin\alpha\,\cos\delta, \sin\delta\right) \tag{20}$$

The core of the pipeline is represented by the Gooding algorithm. It leverages a first guess on the ranges at the boundaries of the observation to build the corresponding position vectors by means of Eq. 19. They are linked through

the solution of a Lambert problem so that initial velocity and, consequently, the complete initial state are obtained. The latter is then propagated through unperturbed Keplerian dynamics, deemed admissible for this first estimate, across every measurement epoch in between the initial and the final ones. The computed intermediate states are then projected onto the angular measurement space to compare them with the actual ones and build $N_{obs} - 2$ residuals. This entire process is wrapped up as a cost function C to minimize the mentioned residuals squared sum by tuning the boundary ranges values:

$$\min_{\rho_0, \rho_{N_{obs}}} C(\rho_0, \rho_{N_{obs}}) \tag{21}$$

Providing this algorithm with a suitable firs guess is crucial to grant convergence to a meaningful solution, so a standard Gauss method-based process has been developed, as described in,[12] to cope with this aspect if a first guess is not given as input to the pipeline. Due to Gauss method limitations in angular span,[13] according to the involved observation width different options are provided:

- With arc span higher than u_b, where u_b can be set by the user as upper bound, two distinct arcs are used to give the corresponding two range guesses. They are built by selecting the portion of the original arc within the selected limit, starting respectively from the first and the last epochs measurements. So two u_b-wide arcs are used to perform Gauss.
- With arc span lower than u_b the entire arc is used to obtain a first guess used as both initial and final range.
- With arc span lower than l_b, where l_b can be set by the user as lower bound, an alert is shown to warn the user of possible inaccurate results

The same method is applied to obtain a backup orbit estimate in case the Gooding method fails in reaching meaningful results. In this instance, a covariance is associated to the computed state by a first-order projection of the input sensor covariance $\mathbf{P_y}$ by means of the transformation Jacobian $\mathbf{J}$ linking measurements to the entire state:

$$\mathbf{P_x} = \mathbf{J}\,\mathbf{P_y}\,\mathbf{J}^T \tag{22}$$

6. Numerical analysis

The numerical validation of ISOC Suite OD tool is here reported. The measurements are simulated considering an optical and a radar stations as baselines. As representative of the former category, Cassini has been chosen: it is an Italian telescope belonging to the EUSST consortium, which is capable of tracking sources in MEO and GEO by mechanically steering its Field of View (FoV), resulting in a very large Field of Regard (FoR).[3] As radar sensor, the Bistatic Radar for LEO Survey (BIRALES) has been selected: it is an Italian bistatic radar system capable of carrying out LEO objects observations in survey mode, that is keeping a fixed pointing direction and gathering signal from sources which cross the FoV.[14]
Optical data were simulated considering a time window of one hour (from the 11 p.m. to the 12.00 p.m.) of April, 29^{th} 2022, while for the radar data the entire day was considered. This choice is linked both to the target visibility in the optical case (only at night) and to the larger FoR an optical telescope can have with respect to the survey radar FoV. Furthermore, a noise was attributed to the sensors:

- BIRALES: 1e-02 deg on the angular track and 100 m on the range
- Cassini: 6e-04 deg on the angular track

Three orbital regimes were considered to compute the satellite passes intersecting the FoV and the FoR of the two stations (the target trajectory was computed through SGP4[5]):

- Low Earth Orbit (LEO): 100 radar passes.
- Medium Earth Orbit: 100 optical passes.
- Geostationary Orbit: 100 optical passes.

Based on this dataset, the software performance are assessed for the correlation, the ROD and the IOD processes as follows. In particular, median position error, median velocity error and median correlation index are used as metrics.

6.1 Correlation process

Concerning the correlation process, for each pass a TDM has been synthetically generated. In addition to the sensor noise described above, observation data are generated by perturbing the observed object initial trajectory according to the uncertainty described in.[15]
The correlation process simulation is carried out by considering a catalogue of 3348 objects, and the main results are reported in Tab. 1, in terms of correlation rate and median correlation index. In the process, an angular filter of 10 deg is used.

Orbital regimen	Correlation rate [%]	Correlation Index
Radar		
LEO	100	0.1509
Optical		
MEO	100	0.1124
GEO	100	0.1684

Table 1: Synthetic data: correlation.

As Tab. 1 shows, the process always correlates the measurements to the correct object, with a median correlation index smaller than 1.

6.2 Refined Orbit Determination

To test the software on the ROD procedure, two situations were considered: the case in which no covariance is linked to the catalogued object information and the case in which it is. In both of them, the first guess was retrieved by perturbing the TLE related to the pass through the covariance given by,[15] the same employed to quantify the uncertainty of an orbital state that is not provided with it, and then propagated towards the observation epochs through an unscented transformation.[6]
In the no-covariance case, the Non-linear Least Squares procedure (described in Sec. 4) is run. In order to reproduce the mismatch between the satellites trajectory and the method exploited in the tool, a keplerian propagator is considered in the batch filter cost function in place of SGP4[5] (which was used to simulate measurements).

Orbital regimen	Pos. Error [km]	Vel. Error [km/s]	Correlation index
Radar			
LEO	2.2e-01	1.5e-02	1.2e-01
Optical			
MEO	1.6e+00	3.5e-04	1.7e-01
GEO	1.0e+00	5.2e-05	1.6e-01

Table 2: Synthetic data: ROD without covariance.

Tab. 2 shows the no-covariance ROD result. The radar case (LEO scenario) shows a position error much smaller than 1 km, while the velocity one is quite remarkable. This is mostly due to the mismatch between the actual target trajectory and the analytical propagation in the filter. Nevertheless, the correlation index is smaller than 1, and this proves the compliance of the ROD procedure result with the measurements.
In the optical case, the error in position increases, while the velocity one decreases. On one hand, the former aspect is due to the absence of the slant range measurement, which does not compensate to the noisy angular track. Nevertheless, it must be to pointed out that, given the scale of MEO and GEO regimes, a position error in the order of 1e+00 km corresponds to a maximum of 0.01% of the orbit radius. On the other hand, the velocity error decrease is due both to the lower velocities the GEO and MEO satellites have, and the less effective perturbations they experience. This latter factor decreases the mismatch between the actual trajectory and the one reconstructed through the analytical propagator (most importantly in GEO), and it implies an error decrease in velocity.
In the covariance case, the UKF[8] was used to update the state sequentially, according to the procedure described in Sec. 4. Analogously to the no-covariance case, a keplerian propagator is used in the filter, whereas the actual target trajectory was computed through SGP4.[5]

Orbital regimen	Pos. Error [km]	Vel. Error [km/s]	Correlation index
Radar			
LEO	7.9e-02	3.6e-04	4.8e-04
Optical			
MEO	8.4e-01	2.2e-04	1.9e-01
GEO	6.2e-01	5.2e-05	1.8e-01

Table 3: Synthetic data: ROD with covariance.

From Tab. 3, the first aspect to stand out is that the error are much smaller than the ones of Tab. 2. This is due to the UKF, which is more robust than the batch filter used in the no covariance case.
More in detail, the LEO position error is smaller than the GEO and MEO ones, while the situation is reversed for what concerns the velocity error. The reasons behind this fact are the same as the no-covariance case, that is the slant range measurement the radar LEO case can take advantage of, the mismatch between the SGP4 and the analytical propagator, and the weaker influence of perturbations in GEO and MEO environments. Overall, the correlation index proves the compliance of the ROD result with the measurements. In particular, it is very small for the radar LEO case.

6.3 Initial Orbit Determination

The IOD procedure is then tested, according to the algorithm presented in Sec. 5.

Orbital regimen	Pos. Error [km]	Vel. Error [km/s]	Correlation index
LEO	5.3e-02	5.4e-03	1.2e-01

Table 4: Synthetic data: radar IOD.

First, Tab. 4 shows the radar IOD results, which are very accurate both in position and in velocity. The former are comparable with the one of the ROD covariance case, while the latter are one order of magnitude worse. This is reasonable, as no orbital state prediction is given as process input.

Orbital regimen	Pos. Error [km]	Vel. Error [km/s]	Correlation index
MEO	2.4e+00	4.2e-04	2.2e-01
GEO	7.2e+00	5.2e-04	2.1e-01

Table 5: Synthetic data: optical IOD.

Concerning the optical IOD, Tab. 5 shows results which are coarser than the radar ones and comparable to those of the no-covariance ROD (Tab. 2). This is mostly due to range estimation, being the first step of the employed methods, and the fact that a Lambert problem is used to link initial and final positions as part of the Gooding estimation process, simplifying the underlying dynamics with respect to the one actually linking measurements across the observation arc. Nevertheless, the error is small compared to the MEO and GEO scales, as observed above about the no-covariance ROD performance in the optical case.

7. Real data analysis

In this section, the performance of the tool is assessed based on real data, which are represented by a radar and an optical observations, of Sentinel-3B (LEO) and Galileo 17c (MEO) respectively, whose orbital parameters are reported in Tab. 6. The latter is carried out by MITE[16] on the February 22^{nd}, 2022, by giving the angular track, while the former by MFDR[17] on the November 24^{th}, 2021, by providing angular track, slant range and Doppler shift. Both of the two sensors belong to the EUSST network. It is important to observe that, even though MFDR is a tracking radar, their measurements are here used also to assess the results of the radar IOD process, which is usually applied to data from surveillance radars.

	a [km]	e	i [deg]	Ω [deg]	ω [deg]
Sentinel-3B	7178.0	0.0012	98.7	33.3	56.8
Galileo 17	29601.9	0.00017	54.9	144.4	266.0

Table 6: Real data: targets orbital parameters.

Based on these data, median position error, velocity error and correlation index are used to asses the results. It is important to point out that the performance here reported include also the effects of the measurements quality.
First, the correlation process is run considering a 12000 objects catalogue (taken from Spacetrack website[18]). In both of cases the measurements result correlated to the correct object, and the correlation indexes are reported in Tab. 7. It is possible to notice that the correlation index for the radar observation is one order of magnitude larger than the optical case one, and this is linked to the measurements quality, as further discussed below.

	Correlation index
Radar	1.8e-01
Optical	3.6e-02

Table 7: Real data: correlation.

Then, the ROD procedure without covariance is tested, starting from the TLEs (available on Spacetrack website[18]) which is closest to the observation epochs. The results are reported in Tab 9, where it is possible to notice that the radar position error is much smaller than the optical on, whereas the velocity errors present a reverse behaviour. The radar correlation index is larger than 1, and this can be linked to the real measurements quality (as mentioned in Sec. 3), in particular to the non-zero mean noise. Overall, the errors are consistent with those shown about synthetic data (Tab. 2), except for the velocity error, which, for the radar case, is better in real data than in the synthetic simulation, while the opposite occurs for the optical observation.

	Pos. Error [km]	**Vel. Error [km/s]**	**Correlation index**
Radar	1.5e-01	2.5e-03	3.8e+00
Optical	2.3e+00	1.1e-03	4.1e-01

Table 8: Real data: ROD without covariance.

The ROD procedure with covariance is also tested, by considering, as prediction, the result of an UT transformation[6] of the TLE with a covariance associated according to.[15] Tab. 9 reports the results of this analysis, and, comparing it to Tab. 3, it is possible to notice that there is a performance deterioration due to the real data quality. It is also evident that the radar shows larger errors than in the no-covariance case, and this is against what observed in synthetic data. This is likely due to the algorithm sensitivity to data quality or to a correspondingly reliable uncertainty. Nevertheless, the results are deemed as sufficiently accurate and support what has been achieved in the synthetic scenarios.

	Pos. Error [km]	**Vel. Error [km/s]**	**Correlation index**
Radar	4.0e-01	2.9e-03	3.6e+00
Optical	1.9e+00	7.5e-04	1.6e-01

Table 9: Real data: ROD with covariance.

Finally, Tab. 10 shows the results of the IOD process. There is a partial deterioration with respect Tab. 4 and Tab. 5 (except for the radar velocity error), but this is still reasonable based on the real data quality.

	Pos. Error [km]	**Vel. Error [km/s]**	**Correlation index**
Radar	1.9e-01	2.0e-03	1.4e+00
Optical	4.1e+00	5.3e-04	6.6e-02

Table 10: Real data: IOD.

To sum up, the analysis shows that the developed algorithm works efficiently even in real case scenario, and the partial deterioration observed does not affect the compliance of the result.

8. Conclusions

This paper presented the orbit determination process embedded in the ISOC Suite. The procedure inputs are the measurements (provided as the TDM format) and the catalogue of orbiting objects, and the process depends on whether the observation data are correlated to a catalogued object, or are not. In this latter case, dedicated methodologies for initial orbit determination were implemented, both for radar and optical measurements. An extensive numerical validation campaign proved the reliability of the suite, which is further confirmed by real data analysis.
In the future, the process will be updated according to new research outcome, and ISOC Suite will be enriched with additional functionalities linked to the orbit determination process.

9. Acknowledgement

The authors are grateful to Leonardo Company for the collaboration in the ISOC Suite realization.

References

[1] ESA Space Debris Office. Esa's annual space environment report. Technical report, European Space Agency, 2022.

[2] Tim Flohrer and Holger Krag. Space surveillance and tracking in esaâs ssa programme. In *7th European Conference on Space Debris*, volume 7, 2017.

[3] European Space Surveillance and Tracking. Eusst service portfolio. Technical report, EUSST, 2021.

[4] Consultative Committee for Space Data Systems. *Tracking Data Message*, ccsds 503.0-b-1 edition, 2007.

[5] David Vallado, Paul Crawford, Ricahrd Hujsak, and T.S. Kelso. *Revisiting Spacetrack Report #3*.

[6] S. Julier, J. Uhlmann, and H.F. Durrant-Whyte. A new method for the nonlinear transformation of means and covariances in filters and estimators. *IEEE Transactions on Automatic Control*, 45(3):477–482, 2000.

[7] Byron D. Tapley, Bob E. Schutz, and George H. Born. Chapter 4 - Fundamentals of Orbit Determination. In Byron D. Tapley, Bob E. Schutz, and George H. Born, editors, *Statistical Orbit Determination*, pages 159–284. Academic Press, Burlington, 2004.

[8] S.J. Julier and J.K. Uhlmann. Unscented filtering and nonlinear estimation. *Proceedings of the IEEE*, 92(3):401–422, 2004.

[9] Jan Siminski. Techniques for assessing space object cataloguing performance during design of surveillance systems. In *6th International Conference on Astrodynamics Tools and Techniques (ICATT)*, pages 14–17, 2016.

[10] David A. Vallado. Chapter 4 - Initial Orbit Determination. In Wiley J. Larson, editor, *Fundamentals of Astrodynamics and Applications*, pages 249–261. McGraw Hill, New York, 1997.

[11] Jeremy Davis Troy A. Henderson, Daniele Mortari. Modifications to the gooding algorithm for angles-only initial orbit determination. In *American Astronomical Society Meeting 238*, 2010.

[12] Howard D. Curtis. Chapter 5 - Preliminary Orbit Determination. In *Orbital Mechanics for Engineering Students*, pages 279–287. Buuterworth-Heinemann - Elsevier, Oxford, 2014.

[13] J.O. Cappellari A.C. Long. Chapter 9 - Launch and Early Orbit Methods. In *Goddard Trajectory Determination System (GTDS), Mathematical Theory*, pages 9–9. Oxford, 1989.

[14] M.F. Montaruli, L. Facchini, P. Di Lizia, M. Massari, G. Pupillo, G. Bianchi, and G. Naldi. Adaptive track estimation on a radar array system for space surveillance. *Acta Astronautica*, 2022.

[15] Tim Flohrer, Holger Krag, and Heiner Klinkrad. Assessment and categorization of tle orbit errors for the us ssn catalogue. 2008.

[16] Giovanni M Del Genio, Jacopo Paoli, Enrico Del Grande, Ferdinando Dolce, Walter Villadei, Marco Reali, and Andrea Aquilini. Italian air force radar and optical sensor experiments for the detection of space objects in leo orbit. In *Proceedings of the Advanced Maui Optical and Space Surveillance Technologies Conference*, volume 1, page 3, 2015.

[17] Detriti spaziali, il contributo di leonardo, vitrociset e telespazio per il monitoraggio e la prevenzione dei rischi. LEONARDO. Accessed 21.04.2022, https://www.leonardo.com/it/news-and-stories-detail/-/detail/space-debris-leonardo-and-vitrociset-and-telespazio-s-contribution-to-risk-monitoring-and-prevention.

[18] Space-track website. Space-track. Accessed 12.04.2022, https://www.space-track.org/auth/login.